AD-A051 518 INSTITUTE FOR ACOUSTICAL RESEARCH MIAMI FLA F/G 8/10
BEAR BUOY: THE MOORING CONFIGURATION MODEL AND METHOD USED TO C--ETC(U)
DEC 77 K L ECHTERNACHT N00014-74-C-0229
UNCLASSIFIED IAR-77008 NL

1 OF 1
AD A051518

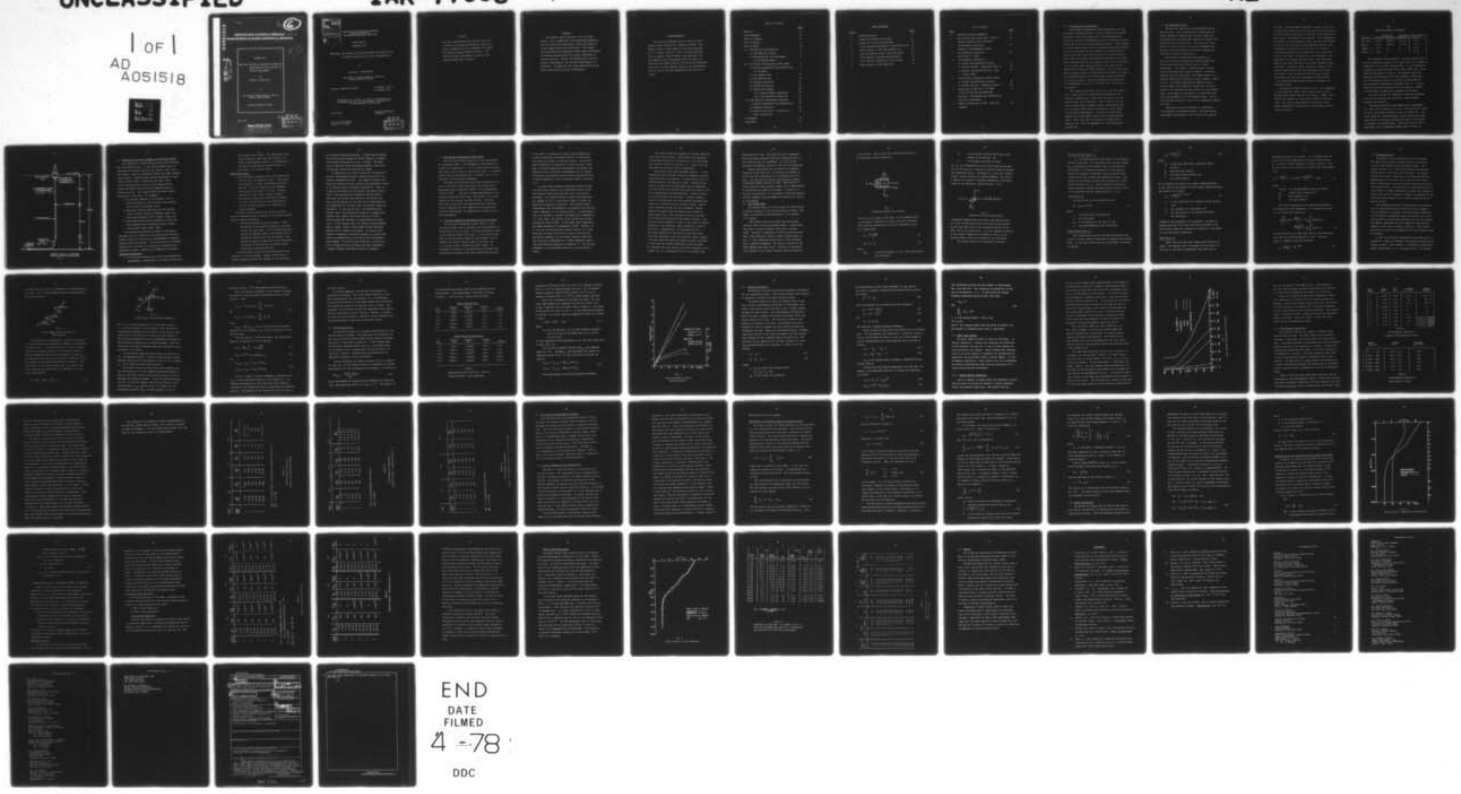

END
DATE FILMED
4-78
DDC

INSTITUTE FOR ACOUSTICAL RESEARCH
MIAMI DIVISION PALISADES GEOPHYSICAL INSTITUTE

December 1977

BEAR Buoy: The Mooring Configuration Model and Method Used to Correct Sensors for Vertical Displacements

by

Kenneth L. Echternacht

to

The Office of Naval Research, Code 222
Sensor Systems Program

Contract: N00014-74-C-0229

IAR 77008

Miami, Florida 33130

INSTITUTE FOR ACOUSTICAL RESEARCH
MIAMI DIVISION OF
PALISADES GEOPHYSICAL INSTITUTE

Final Report

December 1977

BEAR Buoy: The Mooring Configuration Model and Method Used to Correct Sensors for Vertical Displacements

by

Kenneth L. Echternacht

The Office of Naval Research, Code 222
Sensor Systems Program

Contract: N00014-74-C-0229

1 November 1976 to
31 December 1977

IAR 77008

Morton Kronengold,
Director

615 S.W. 2nd Avenue
Miami, Fla. 33130

N O T E

The work reported here was carried out at the Institute for Acoustical Research, Miami Div., from 1 November 1976 to 31 December 1977 under ONR Contract Number N00014-74-C-0229. "No inventions were conceived or first put into practice under this contract".

ABSTRACT

This report constitutes Part 2 of a two part report. Part 1 "BEAR Buoy: The Engineering Documentation for Scientific Application", dealt with details of the system design and calibration. This report first develops the mathematical model used to determine the mooring configuration for varying conditions of external forcing. Second, the method used to correct sensors (thermistors) for vertical displacements is presented. Included are case study comparisons of the model predictions vs actual measurements.

ACKNOWLEDGEMENTS

This work was supported by the Office of Naval Research under Contract No. N00014-74-C-0229. The author wishes to acknowledge the following persons: Dr. A.O. Sykes, Code 222, Office of Naval Research, for his support; Robert Marema, Raul Murciano, and the members of the engineering staff for their co-operation and support both in the field and laboratory; David Smith of the computer section; and James Nangle and the crew of the R/V GULFQUEST during the field phases.

Table of Contents

List of Figures

List of Tables

1.0 Introduction and Background

Oceanographic measurements from moored buoys are contaminated by mooring motion. Previous studies (eg, Wunsch and Dahlen, 1974) have shown that deep instrumentation located on surface buoyed mooring lines can undergo vertical excursions as large as several hundred meters. Large changes in sensor depth result from low frequency horizontal meanderings of the surface buoy and changes in configuration of the mooring line under the action of the surface forces of wind, wave, and current and subsurface drag due to current. High frequency motions are present as well due to the motion of the surface wave field and due to line strum on the mooring line caused by vortex shedding. For an operational moored system a model is needed which can predict the motion and configuration of the mooring under varying conditions of external forcing. Given the predicted configuration the measurements can then be corrected for vertical displacements.

This report constitutes Part 2 of a two part report. Part 1 "BEAR Buoy: The Engineering Documentation for Scientific Application", dealt with the details of the system design and calibration. Part 2 details the analytical model used to predict mooring configuration and the auxilliary model used to correct the sensor signal for vertical displacements. Included are case study comparisons of the model predictions vs actual measurements. These were used to validate the model and to establish the limits of ambiguity for the displacement corrections.

1.1 The BEAR Buoy System

The buoy was fabricated from two NAVAIR cruiser mooring buoys. The two buoys were strengthened and welded together to provide the internal volume for instrumentation and additional buoyancy to support the thermistor string and mooring. The buoy has a total weight of 13061 Kg and is filled with expanded polyurethane foam which provides a positive buoyancy of 10715 Kg per meter of buoy draft.

Buoy motion was measured and recorded by a separate on-board recording data system supplied by the National Data Buoy Office, Bay St. Louis, Mississippi. The system - Portable Ocean Platform Motion Instrumentation Package (POPMIP)- is battery operated and self-contained. The POPMIP remains in a stand-by mode until activated by radio command. After turn-on, the system sequentially samples each of 6 analog sensors 3.82 times per second over a turn-on interval of 2 minutes and then returns to the stand-by mode. Each sample is converted to a three-digit BCD word and recorded on 1/4 inch magnetic tape. The internal format provides a total of 90 independent samples per tape.

The mooring sensors included the tensiometer, inclinometers, and pressure gauge. The strain gauge tensiometer was mounted in the clevis at the base of

the buoy. The tensiometer provided a measure of the sum of the forces acting on the buoy due to the surface forces of wind, current, and waves, to the sum of the subsurface drag, and to the weight of the mooring. Two inclinometers were mounted on the thermistor cable: one near the surface and one at the lower end of the thermistor string. The inclinometers were filled with silicon oil of 60,000 centistoke viscosity in the upper unit and 30,000 centistoke in the lower, resulting in a time constant of approximately 60 seconds for both units. This served to damp out the major portion of the higher frequency cable vibration. A pressure gauge located at a depth of 650 meters flooded during the buoy deployment and was not operational. The information from the strain gauge tensiometer and the two inclinometers provide inputs to an analytical model which was used to estimate the thermistor depth.

The mooring system as shown in Fig. 1 was comprised of the thermistor cable, nylon mooring line, and the ground tackle (chain sections and anchor). Table 1 summarizes the lengths of each section under no-load and load. The static load includes the stretch of each member computed for conditions of zero surface and subsurface forcing.

Table 1

BEAR Buoy Mooring Components

Section	Length (m) Unstretched	Length (m) Static Load	Percent Stretch	wt/unit length (Kg m^{-1})
T. cable	1924.4	1933.8	0.49	1.69
Nylon	2713.6	2821.1	4.00	0.14
Chain - 1	137.2	-	-	15.54
Chain - 2	384.0	-	-	25.75

The thermistor cable comprised the upper portion of the mooring system and consists of an inner core of 37, number 18 conductors in a wet core configuration. It is protected by a double lay torque balanced steel armor cable with a rated breaking strength of 33,000 kg. The armored cable was mechanically connected to the buoy through a clevis and then led through a pipe to the top of the buoy where it was connected by waterproof connectors (Fig. 1). Plastic ribbon fairing was interwoven into the armor to a depth of 1000 meters to reduce the strumming of the cable.

The lower end of the thermistor string was connected to a 2-inch nylon mooring line with a rated breaking strength of 41,000 kg.

The lower end of the nylon mooring line terminated in 5 shots (27.4 m/shot) of 1 1/8 in. stud link and 14 shots of 1½ in. buoy chain weighing a total of 12020.1 kg. The chain acted as a varying dynamic load for the mooring and also served to virtually increase the scope of the anchor to maximize its holding power. The anchor was an 1800 kg Navy-type, with an expected holding power of 5400 kg.

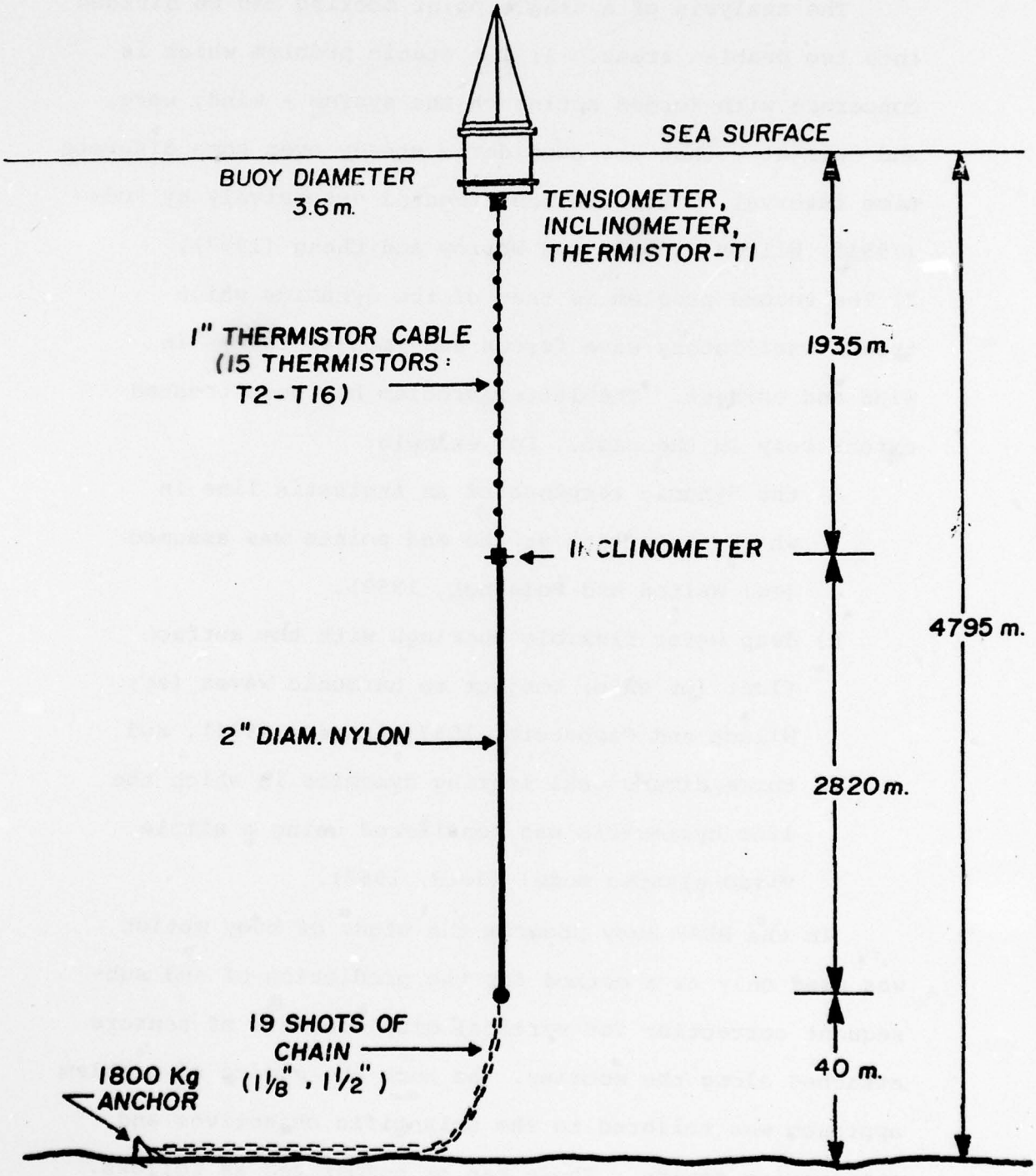

BEAR BUOY SYSTEM

Fig. 1

1.2 Background for the Development of the Mooring Model

The analysis of a single point mooring can be divided into two problem areas. 1) The static problem which is concerned with forces acting on the system - wind, wave, and current - that are considered steady over some discrete time interval. This has been treated extensively by Pode (1951), Wilson (1961), and Morrow and Chang (1967). 2) The second problem is that of the dynamics which treats oscillatory wave forces and impulse forces in wind and current. The latter problem has been treated extensively in the past. For example:

a) the dynamic response of an inelastic line in which the motion at the end points was assumed (eg; Walton and Polachek, 1959),

b) deep water flexible moorings with the surface float (or ship) subject to harmonic waves (eg; Wilson and Garbaccio, 1967; Langer, 1964), and

c) three dimensional mooring dynamics in which the line hysteresis was considered using a simple visco-elastic model (Reid, 1968).

In the BEAR Buoy program the study of buoy motion was used only as a method for the prediction of and subsequent correction for vertical displacements of sensors attached along the mooring. As such the choice of problem approach was tailored to the scientific objectives and engineering design. These can be summarized as follows.

Scientific objectives:

1. To study the internal wave field using temperature measurements (thermistors) as a means of detecting

the internal wave signal. The thermistors were spaced along the cable from near surface to a depth of approximately 1800 m. The emphasis is the study of long period internal waves, in particular, the internal tides.

Engineering Design:

1. The individual thermistor units were potted and spliced into the thermistor cable. Each splice was encased in a steel, egg-shaped protective housing. The time constant of the imbedded sensor was of the order of 13 min., slightly greater than the 12 min. sampling interval.
2. The mooring sensors were mechanically damped to filter out surface wave generated motions as well as high frequency line strum due to vortex shedding.

The above design features were used to minimize signal contamination due to motions at frequencies higher than the sampling interval.

3. The mooring design was the following. Under conditions of zero external forcing a non-zero tension was maintained. With increased external forcing the dynamic load on the mooring was increased by lifting chain off the bottom. This served to reduce the magnitude of the horizontal excursions of the buoy and to prevent exotic curvatures in the mooring line.

Given the above criteria the mooring analysis was treated as a static problem. Dynamic effects due to higher frequency motions were assumed to be eliminated

by the above engineering design. A model was developed which utilizes the method of finite elements to compute the mooring configuration in an x,z plane. The model uses as explicit inputs prescribed boundary conditions and external forcing on the mooring system.

In application the sensor signal was corrected for vertical displacements using a modified version of the mooring configuration model. The modified version computes the external forcing (surface and subsurface) acting on the system using the measured quantities - cable inclination and tension at the surface and cable inclination at the bottom of the thermistor string (1825 m). Given the inclination and tension at the surface the total surface forcing on the buoy can be determined but the components due to wind, wave, and current cannot be separated. In the initial pass, the method uses the surface input (inclination and tension) to compute the surface force (total) and solves the set of force-balance equations assuming a no-subsurface drag condition. If the solution does not converge then subsurface drag is added. Under a drag condition the horizontal tension is not constant with depth. As such the difference in measured inclination between the surface and 1825 m is proportional to the sum of the drag between those depths. To satisfy this condition a current profile is computed which satisfies the drag requirement. A simple linearly- decreasing profile is assumed.

2.0 The Mooring Configuration Model (MCM)

This section treats the details of the development of the mooring model. The mathematical description includes the formulation of 1) the surface forces of wind, wave, and current acting on the surface buoy, 2) the subsurface drag on the mooring due to current, and 3) the elasticity of the mooring components.

The model was evaluated using data collected at the time of the buoy implant and during the Ground Truth Experiment (GTE) conducted in April, 1976 (Echternacht, 23 March 1976). The data included measurements of the surface conditions (wind, wave, and current), the total tension on the mooring, and XBT profiles. The data were used to evaluate the predicted mooring configuration by comparing the buoy temperatures corrected for vertical displacements as computed by the model vs the XBT measurements.

2.1 General Assumptions and Capabilities of the Model

The mooring configuration model (MCM) is a two dimensional model used to determine the configuration of the mooring in an x-z plane. The model requires as input 1) the buoyancy force on the buoy, 2) the surface parameter (wind and current speed and wave height) used to compute the surface forces acting on the buoy, and 3) a current profile through the water column. As discussed in Section 1.2 the mechanical and sensor subsystems were designed to low pass signals with periods

of the order of minutes and longer thus eliminating or at least minimizing the dynamic motions of the surface wave field and surges in wind and current. As such the model formulation is treated as a static problem. When used to correct temperature measurements for signal contamination due to vertical displacements of the sensors the mooring configuration for each data acquisition time is solved separately (to be explained further in Section 3.0).

An earth fixed Cartesian coordinate system is used with the origin placed at the undisturbed level of the free surface (buoy mean waterline) and z is positive downwards. All external forces, surface and subsurface, are assumed to act in a horizontal plane in either the positive or negative x-direction. The mooring sensors (tensiometer and inclinometers) only measure the resultant scalar components of the applied forces. No instrumentation was included to resolve individual force components; i.e, wind, wave, and current at the surface and current through the water column. In the model these components are added separately as independent forces. However, as in the case of the horizontal surface forces, it is the resultant of these forces that is used to specify the horizontal component of the surface boundary condition. The resultant is expressed as a vector component: amplitude and direction (positive or negative x). The vertical component, to be discussed further on, is the buoyancy force.

The surface waves are assumed to be small amplitude, deep water gravity waves. Wave period and subsequent displacement motions of the buoy due to the wave field are neglected (refer to Section 1.2). Hence, only the amplitude of the wave field is considered.

All mooring lines are considered elastic. In the formulation the nonlinear elasticity dependent on prior loading history is neglected. A stress-strain curve is derived based on the percent of load. Different load curves are used for the individual mooring components. The load curves were derived using data from static load tests conducted by the manufacturers. Dynamic effects on the load curves are neglected. Internal damping forces in the mooring lines are assumed negligible compared with viscous drag and stiffness forces. Hydrostatic pressure forces are not considered. Sensor packages attached along the mooring are treated as added weight only. The thermistor units are encased in 15 protective cylindrical egg-shaped housings. The maximum housing diameter (0.1016 m) and length (0.3483 m) compared to the thermistor cable dimensions (0.0252 m and 1924 m, respectively), is considered to be a negligible addition to the total viscous drag force. Since the thermistor units are spaced at nearly regular intervals along the cable the housing weights are added to the total and evenly distributed along the cable. No allowance for line creep of the nylon component is included, but it is recognized that it is possible over

long periods of time. The cable and nylon components used were torque balanced such that elongations due to line rotation are not considered. All wave forces (exciting and damping) acting on the line are neglected.

Viscous drag forces due to current are computed using the square drag law. The forces are assumed to act on the line cross-section in the direction of the flow. For the buoy the wetted cross-section is used. A sectioned current profile is used. Each section is linear but most actual profile shapes can be approximated by increasing the number of sections. A total of n-1 sections is possible; n is the number of mooring elements. To save computer time the number of sections are limited to ten maximum.

2.2 The Surface Buoy

The surface buoy has a total weight of 13061 Kg and a positive buoyancy of 10715 Kg per meter of draft. The shape is cylindrical with dimensions: 3.6 m diameter, 2.7 m length.

The forces acting on the buoy are the surface vertical force and the horizontal forces - viscous drag force due to surface current, wind force, and wave force. The buoy is modeled as a rigid surface piercing body. The coordinate system is shown schematically in Fig. 2. The coordinate system used is fixed Cartesian with z positive downwards. The origin is placed at the mean computed buoy water line. The buoy is considered to be upright at all times (vertical buoy axis parallel

to the z-axis). The x-axis is by convection positive in the downstream current direction.

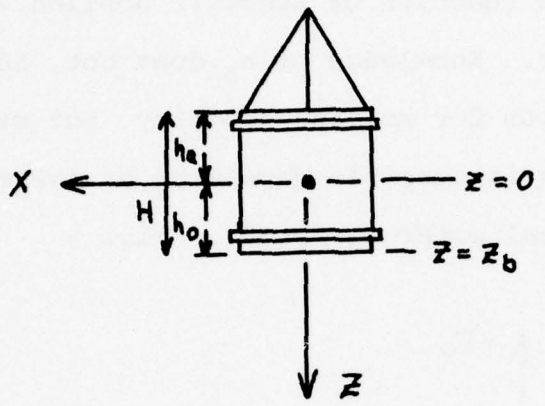

Fig. 2

Coordinate System for the Buoy

H is the total length of the buoy, h_o the computed draft, z_b the depth of penetration, and h_a the buoy freeboard. The following expressions are used to determine h_o and h_a, respectively.

$$h_o = \frac{Fv - Mg_b}{B} \tag{1}$$

$$h_a = H - h_o \tag{2}$$

where

Mg_b is the buoy weight in air, g the acceleration due to gravity,

F_v is the surface vertical force due to the weight of the mooring, and

B the buoyancy per meter of draft.

Eq. (1) is an expression for the static equilibrium position of the buoy as a function of specific applied surface and subsurface forces. Knowledge of h_o does not, however, yield a unique solution for mooring geometry, but rather a family of solutions is possible depending on the magnitudes of the individual external forces. Fig. 3

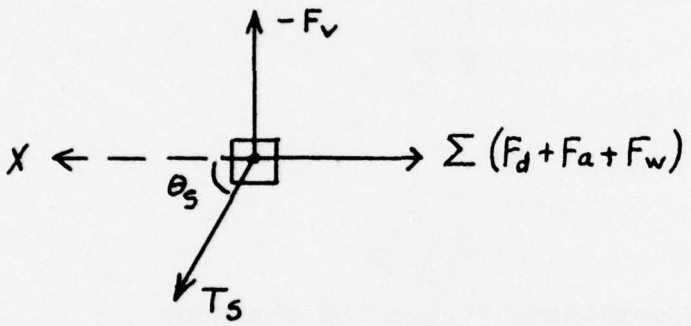

Fig. 3
Condition of Static Equilibrium

illustrates schematically the static equilibrium state. F_d is the viscous drag force due to the surface current, F_a the wind drag force on the freeboard portion of the buoy, and F_w the wave force. T_s is the tangential tension at the surface imparted by the mooring and θ_s is the surface tension angle with respect to the horizontal.

The surface forces are formulated as follows.

Surface vertical force, F_v

F_v, is effectively the total weight of the mooring acting on the buoy. For the static case the buoy weight, Mg_b, is balanced by the buoyancy term, B (principle of Archimedes). As outlined in Section 1.2 the mooring system was designed to provide a non-zero tension under conditions of zero surface and subsurface forcing. The details of the design criteria are provided in a latter section (Section 2.6.1). Under conditions of zero external forcing a minimum vertical surface force of 4270.0 Kg is maintained and the minimum draft is 1.62 m.

Wind force, F_a

The wind force, F_a was calculated using:

$$F_a = K \rho_a A \left(Va^2 \right) \tag{3}$$

where,

A is the dry buoy cross-section,

V_a the wind speed,

ρ_a is the density of air (Kg m^{-3}) and

K the non-dimensional drag coefficient.

Viscous drag force, F_d

The viscous drag force on the buoy and mooring line follow a velocity square relationship (Casarella and Parsons, 1970). In the case of the buoy the relationship is written as follows.

$$F_d = \frac{C_d \rho A V^2}{2} \qquad (4)$$

where,

C_d is the drag coefficient, generally taken as unity,

ρ mean sea water density,

A the wetted cross-section, and

V the current speed

Eq (4) defines the form of the normal loading function. In the case of the mooring line the normal loading relationship used is as follows.

$$F_d = \frac{C_d \rho DS V^2 \sin \theta}{2} \qquad (5)$$

D is the cross-sectional diameter of the mooring line,

S the increment of line length, and

θ the inclination of the mooring line from the horizontal.

Tangential drag components are neglected. As shown by Hartman and Nash (1975) from test data collected in the Gulf Stream tangential loadings are generally of the order of 2% of the normal components.

Wave force, F_w

Wave forces are much more complex and difficult to model. The approach was to represent the wave force on the buoy as the sum of hydrodynamic drag and inertia

components acting on a cylinder. It is assumed that the waves are of small amplitude, deep water gravity waves; ie, the ratio of wave amplitude to length $a/L << 1$. Thus the wave force can be written as follows (Dean and Hartman, 1968).

$$F_w(t) = \frac{\rho g C_D D}{4} a^2 \cos^2 \sigma t - \frac{\rho g C_m \pi D^2}{4} a \sin \sigma t \qquad (6)$$

where,

C_D and	are the hydrodynamic drag and inertia
C_m	coefficients, respectively,
ρ	water density, and
D	the buoy diameter

The above expression can be simplified further by eliminating the time dependency. By averaging over time Eq. (6) becomes the following.

$$\frac{1}{T}\int_0^T F_w(t)dt = \frac{\rho g C_D D}{4} a^2 \frac{1}{T}\int_0^T \cos^2 \sigma t \, dt - \frac{\rho g C_m \pi D^2}{4} a \frac{1}{T}\int_0^T \sin \sigma t \, dt \qquad (7)$$

The first term on the right hand side is the mean square value and the second integrates to zero. The wave force is computed using the following.

$$F_w = \frac{\rho g C_D D}{4} \frac{\overline{\quad}}{a^2} \text{RMS} \qquad (8)$$

2.3 The Mooring Line

The mooring line is comprised of three sections. The upper section which connects directly to the buoy is the 1-inch diameter steel thermistor cable. The center section is a 2- inch nylon mooring line and the bottom section 1-1/8 inch stud link chain. It should be noted that under conditions of zero external forcing approximately 42 m of chain are lifted off the bottom. During conditions of non-zero external forcing the static load increases due to the lifting of additional chain off the bottom. The model formulation includes the changes in static load and the subsequent changes in elongation of the nylon and cable members due to varying conditions of external forcing.

The mathematical model of the statics of the mooring line is formulated using the method of finite elements. In that approach, the mooring line differential equations are integrated incrementally down the mooring line to obtain the static equilibrium position for each line element. The spatial coordinate of each element is computed with respect to the origin located at the buoy. The viscous drag force on each line elemement due to the velocity field is included.

In the finite element formulation the mooring line is reduced to a number of straight line segments joined at end points or nodes. Each segment is considered an extensible cable without mass; i.e., a straight spring. All forces

and mass along the cable are assumed to be concentrated at the nodes. Fig. 4 shows schematically the representation of the mooring line.

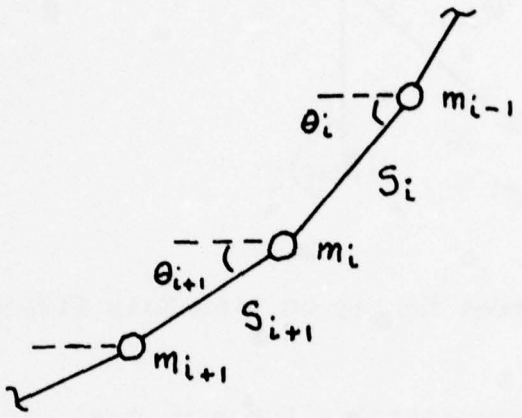

Fig. 4

Finite Element Formulation of the Mooring Line

To illustrate the formulation, consider the balance of forces acting on a differential element of the mooring. As shown in Fig. 5 the line forces are: (1) the constant force due to gravitation and (2) the variable tension forces transmitted from adjoining elements, T_i and T_{i+1}. The constant force due to gravitational attraction is the wet weight per unit stretched length of element i. The fluid force is the viscous drag force, F_{di}, due to the fluid velocity as given by Eq. (5) (Section 2.2). For static equilibrium:

$$T_i + F_{di} + (mg)_i + T_{i+1} = 0 \qquad (9)$$

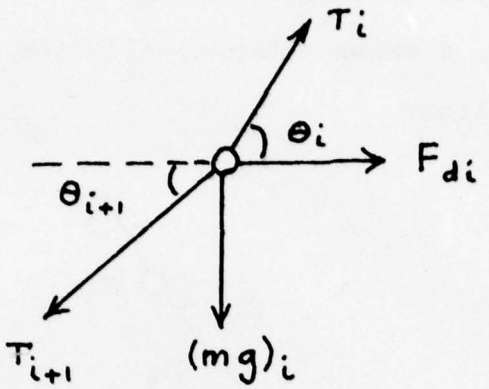

Fig. 5

Forces Acting on Line Mass Element (i)

Eq. (9) is solved sequentially for each mass element i; i = 1 at the surface, n at the bottom. Near the surface the dominant component of the tension is the vertical component due to the weight of the mooring below element i. With increasing depth the vertical component decreases and the horizontal component due to drag increases. Near the bottom the horizontal component dominates resulting in near horizontal line angles.

The horizontal component due to drag, as given by Eq. (5), is computed using $\overline{V}_i$. Here $\overline{V}_i$ is the average current magnitude acting on the differential length of line element, S_i. $\overline{V}_i$ is taken from the current profile.

The tensile forces acting on the n mass elements and the inclination of the line elements change with depth to keep all the above forces in equilibrium (refer to Fig. 5). Consider the following example. Given the equilibrium position, $\hat{Y}_i$, of the ith element, then the inclination of the tension vector, T_{i+1}, acting on the ith element and the equilibrium position, $\hat{Y}_{i+1}$, of mass element i+1 can be

found as follows. $\hat{Y}$ is the geometric position vector.

Since the vertical component of the tension is simply the weight of that portion of the mooring acting on mass element i, then

$$F_{v,i+1} = T_s \sin \theta_s - \int_{j=1}^{i} (mg)_j \, dz$$

and (10)

$$F_{h,i+1} = T_s \cos \theta_s + \int_{j=1}^{i} F_{dj} \, dz$$

where,

$F_{v,i+1}$ and $F_{h,i+1}$ are the vertical and horizontal components of the tension, T_{i+1}, and T_s the tension at the surface (buoy).

Thus the tension, inclination angle, and equilibrium position of element i+1 are as follows.

$$T_{i+1} = \left(F_{v,i+1}^2 + F_{h,i+1}^2\right)^{\frac{1}{2}} \tag{11}$$

$$\theta_{i+1} = \tan^{-1} \left(F_{v,i+1} / F_{h,i+1}\right) \tag{12}$$

and

$$Y_{x,i+1} = Y_{x,i} + S_{i+1} \cos \theta_{i+1}$$

$$Y_{z,i+1} = Y_{z,i} + S_{i+1} \sin \theta_{i+1} \tag{13}$$

Here x, z refer to the x,z component directions and S_{i+1} is the unstretched length of line element i+1. It should be pointed out at this time that line stretch is included in the formulation used to determined the geometric position. The details of the formulation will be given in

the next section.

To briefly summarize, the mooring configuration is determined as follows. The force balance equation is computed sequentially for line elements i=1, n to determine the equilibrium position of each mass element thus describing the geometrical shape of the mooring in an x,z plane. The advantage of this method is that the equations can be derived directly from Newton's Laws of motion. However, it should be noted that this method is limited to static problems with prescribed boundary conditions and external forces.

2.4 Mooring Elasticity

To accurately predict the mooring configuration the line stretch must be included. The elasticity of the mooring for the cable and nylon sections under varying load was included explicitly in the model formulation. It was assumed that the materials followed Hooke's Law; ie., the extensibility of the mooring line is proportional to the pulling on the line due to tension. Extensibility by squeezing due to hydrostatic pressure was not considered.

Having determined the tension acting on the i+1 element of line (Eq. 11) the elastic stretch is calculated as follows. From Hooke's Law the incremental stretch, ΔS_{i+1}, is defined as:

$$\Delta S_{i+1} = \frac{(T_{i+1})\ (S_{i+1})}{\lambda_B} \qquad (14)$$

λ_B is the modulus of elasticity with dimensions of force per unit cross-sectional area, A; ie, $\lambda_B = A \cdot \lambda$. The modulus λ

was determined from static bench tests conducted by the manufacturers. The manufacturers' test data are given in Table 2. For the nylon, eight strand pli-moor

Double Armored Cable

% Load	Tension (Kg)	Modulus, λ_c	Stretch (m)	% Stretch
3.5	1104.1	4.5×10^5	6.0	.31
6.7	2268.0	8.1×10^5	6.8	.36
20.0	6804.0	1.2×10^6	13.7	.71
33.6	11339.9	1.6×10^6	17.2	.89
43.0	14601.0	1.7×10^6	21.0	1.09

Eight Strand Pli-moor Nylon

% Load	Tension (Kg)	Modulus, λ_N	Stretch (m)	% Stretch
2.0	834.6	7.59×10^3	99.4	3.66
5.0	2086.5	1.02×10^4	172.8	6.37
10.0	4173.1	1.23×10^4	294.1	10.84
15.0	6259.6	1.37×10^4	397.1	14.64
40.0	16692.4	2.25×10^4	640.9	23.63

Table 2

Manufacturer Bench Test Data - Load vs Percent Stretch: Cable and Nylon

construction, λ varies from 7.6×10^3 at 2% loading to greater than 2.2×10^4 at leading greater than 40%. For the double armored conductor cable λ varies from 4.5×10^5 at 3.5% loading to greater than 1.6×10^6 at loads greater than 43%.

Values for the modulus λ for both the cable (λ_c) and nylon (λ_N) members were computed from the test data in one percent intervals over the ranges given in Table 2. The values for λ_N and λ_c are shown in Fig. 6. In the model λ was computed as follows, (1) Percent load was computed for each line element i using:

$$\% \text{ Load} = (T/LC) \cdot 100 \tag{15}$$

where

LC, the load constant, is the rated breaking strength - 3.385×10^4 Kg for the cable and 4.173×10^4 Kq for the nylon.

(2) the appropriate λ corresponding to Eq. (15) was found using a table look - up.

Given λ the incremental stretch, ΔS_{i+1}, was computed using Eq. (14). Once ΔS_{i+1}, was determined the element coordinates (given by Eq. 13) were corrected to include the stretch.

$$\begin{aligned} Y'_{x,i+1} &= Y_{x,i+1} + \Delta S_{i+1} \cos \theta_{i+1} \\ Y'_{z,i+1} &= Y_{z,i+1} + \Delta S_{i+1} \sin \theta_{i+1} \end{aligned} \tag{16}$$

The prime denotes the stretch included coordinate.

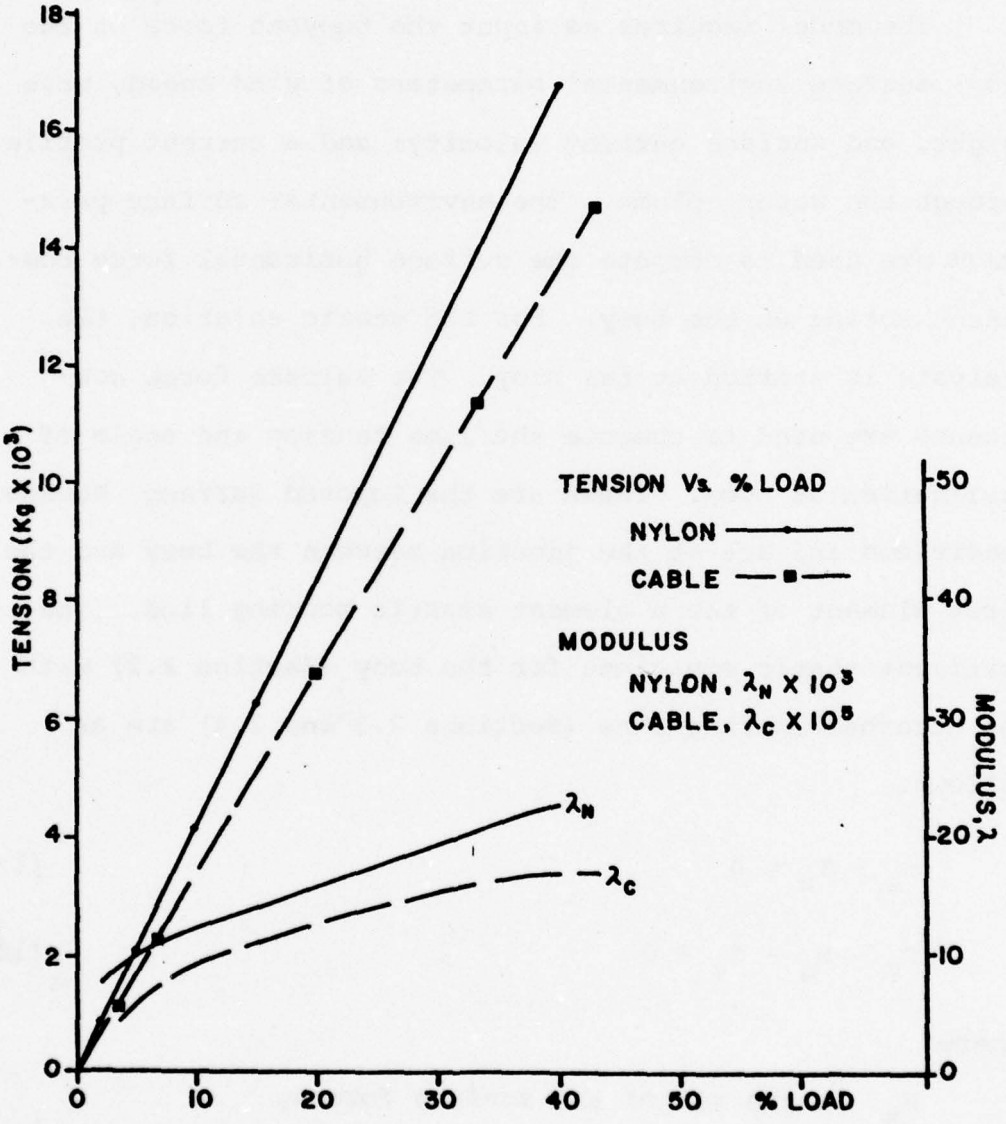

Fig. 6

Load and Modulus Curves:
Nylon and Cable

2.5 Method of Solution

The previous sections outlined the necessary ingredients for the mathematical model. This section details their useage in obtaining a solution for given external inputs.

The model requires as input the buoyant force on the buoy; surface environmental parameters of wind speed, wave height, and surface current velocity; and a current profile through the water column. The environmental surface parameters are used to compute the surface horizontal force component acting on the buoy. For the static solution, the analysis is started at the buoy. The surface force components are used to compute the line tension and angle of inclination at buoy. These are the imposed surface boundary conditions and act at the junction between the buoy and the first element of the n element elastic mooring line. The pertinent static equations for the buoy (Section 2.2) with the attached mooring line (Sections 2.3 and 2.4) are as follows.

$$F_x - T_x = 0 \tag{17}$$

$$F_v - M_g - T_z = 0 \tag{18}$$

where

F_x is the sum of the surface forces,

$F_d + F_a + F_w$, and

M_g is the weight of the mooring.

By specifying F_x we have three unknowns: F_v, M_g, and T_z. Initially, we assume a value for the surface vertical force, F_v', where,

$$F_v' = F_v - M_g \tag{19}$$

Thus the unknowns can be solved using the following,

$$\theta_s = \tan^{-1} (F_v'/F_x) \tag{20}$$

$$T_s = (F_x^2 + F_v'^2)^{\frac{1}{2}} \tag{21}$$

and

$$T_z = T_s \sin \theta_s \tag{22}$$

The subscript s denotes surface parameters.

Having solved the buoy force the mooring line is analyzed next. For the mooring line formulation, a numerical integration is carried down the line in a set of n finite segments. In this representation the line equations can be written as follows.

$$F_{x,i} - T_{x,i} - F_{di} = 0 \tag{23}$$

$$F_{v,i} - mg_i - T_{z,i} = 0 \tag{24}$$

F_{di} is the current drag on element i computed from the current profile.

Solving the force balance equations, (23) and (24), for element i the conditions for the i+1 element are specified as follows.

$$T_{i+1} = (F_{v,i}^2 + F_{x,i}^2)^{\frac{1}{2}} \tag{25}$$

$$\theta_{i+1} = \tan^{-1} (F_{v,i}/F_{x,i}) \tag{26}$$

The coordinate position of each element is found using Eqs. (13) and (16). The iteration is carried out to the end of the mooring; i = n. At that point the bottom boundary conditions should be met, such that:

$$F_{v,n} = 0$$

and

$$\sum_{i=1}^{n} Y'_{z,i} = \xi Z' \qquad (27)$$

Z' is the measured depth = 4793 m, and

ξ = 0.001.

Thus if the computed depth does not agree to within 0.1% the process is repeated with a new F_v' specified.

2.6 Model Case Studies

The model (MCM) was used to study the following. (1) Implant simulation - studies were conducted for conditions of zero-external forcing over a range of water depths and varying mooring line lengths. These studies were conducted prior to the buoy implant to determine the optimum mooring length for the anticipated range of bottom depths. (2) Environmental simulation - these studies were run to determine the mooring configuration under varying conditions of external forcing by the environment.

2.6.1 System Implant Simulation

Prior to implant a bottom survey was conducted to determine the depth of bottom and changes in bottom topography within the proposed study area. The implant site was

located on the abyssal plain approximately 15 Km seaward of the continental margin at a depth of approximately 4800 m. The bottom is relatively flat with minor topographic variations - of the order of a few meters. The mooring design was intended as a semitaut system with a non-zero minimum tension (refer to Section 1.2). To achieve this the design specified that a short section (of the order of tens of meters) of ground tackle (chain) would be maintained off the bottom under conditions of zero - external forcing. As such a knowledge of the mooring configuration under these conditions was necessary in order to specify the lengths of the mooring members (cable and nylon).

Using the MCM a number of case studies were run. The cases included (1) varying the bottom depth with mooring lengths held constant and (2) varying mooring lengths with depth held constant. The results of all case studies will not be presented only the case representing the final mooring specification and measured depth at the implant site.

The input specifications for the final case were the following: (1) bottom depth - 4800 m, (2) cable length - 1924.4 m, and (3) nylon length - 2713.6 m. Fig. 7 illustrates the results. In the figure, $\Delta Z = 0$ represents the depth - 4800 m. For this implant depth approximately 42 m of chain are maintained off the bottom with a minimum non-zero tension of approximately 4270 Kg. It should be noted that stretch in the nylon and cable members was included as shown in the figure. The final mooring lengths as specified by this case study allowed a safety margin of approximately

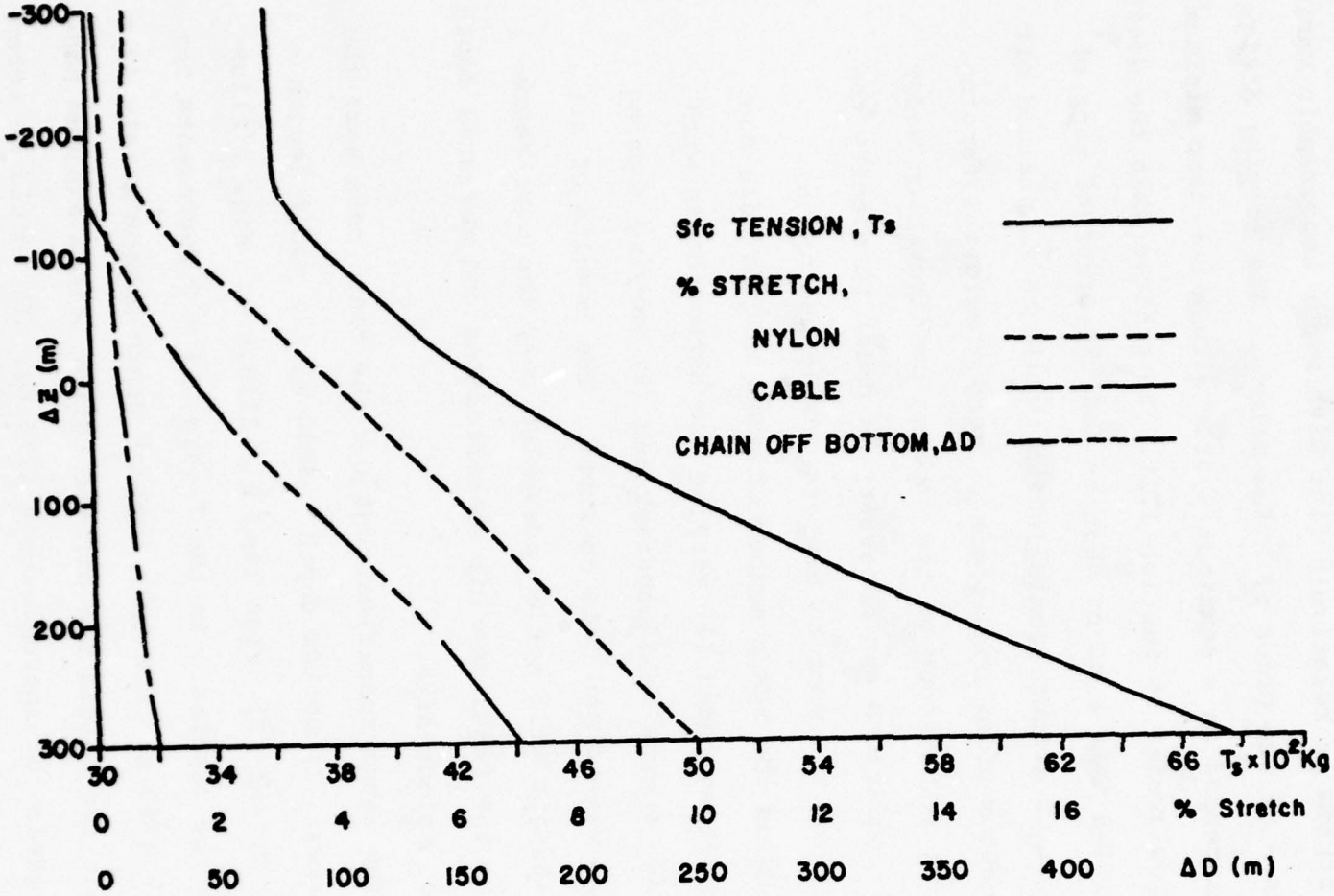

Fig. 7

Final Implant Configuration Simulation

145 m in the depth at the implant site. The results of the case study and thus the MCM calculations were verified at a later date by measuring the weight of the mooring.

During the Ground Truth Experiment conducted in April, 1976 (Echternacht, 23 March 1976) the mooring weight was measured. The sea and weather states were calm. The method entailed hauling on the mooring until the buoy tensiometer was zero and maximum on the hauling tensiometer. The mooring weight - measured tension - agreed with the total calculated model line weight - thus line length - within the error limits of the instrumentation used.

2.6.2 Environmental Simulation

This section presents the results of specific case studies using the MCM. The case studies to be presented represent a wide range of external forcing by the environment. The cases presented are separated into three categories: surface forcing in the presence of a current - linearly decreasing with depth and with shear - and surface forcing in the absence of a current. The above categories were used, in part, to assess the effect of subsurface drag on the mooring. The application of those results are contained in a latter section which details the formulation of the model used to correct sensors (thermistors) for vertical displacements.

Table 3 lists the three case study categories and the magnitudes of the environmental inputs. Within each category the inputs represent conditions of strong, moderate, and mild forcing covering the range of expected sea and weather states

Case Study	Wind (ms^{-1})	Wave (m)	Current sfc (ms^{-1})	Current Profile
1	10.30	3.05	1.03	1.03 - 0.
2	6.90	2.00	.66	.66 - 0.
3	3.50	1.00	.33	.33 - 0.
4	10.30	3.05	0.	0.
5	6.90	2.00	0.	0.
6	3.50	1.00	0.	0.
7	5.00	2.00	1.03	1.03-(-.5)(2500) (-.5)-0. (4793)
8	5.00	2.00	.50	(.5)-(-.5)(2500) (-.5)-0. (4793)
9	5.00	2.00	0.	0.-(-.5) (2500) (-.5)-0. (4793)

Table 3

Environmental Simulation -

Summary of Environmental Inputs

	Depth Zone (m)	T-Range (^{o}c)	Gradient γ_T ($^{o}c/m$)
1	0 - 300	22.6 - 18.4	.014
2	300 - 540	18.4 - 15.2	.013
3	540 - 840	15.2 - 8.0	.024
4	840 - 1000	8.0 - 6.0	.012
5	1000 - 1200	6.0 - 4.6	.007
6	1200 - 2000	4.6 - 3.8	.001

Table 4

Environmental Simulation -

Depth Zones: T vs γ_T

with the exception of rare events such as hurricanes. Cases 1-3 and 7-9 differ in the type of current profile used. The former uses a linearly decreasing profile with surface maximum; the latter includes a current shear (variable) under conditions of moderate surface forcing.

In order to evaluate the effect of external forcing for the various cases the vertical displacement of reference sensors within specified zones was used. The depth zones, as given in Table 4, correspond to regions of nearly constant vertical temperature gradient, γ_T. The γ_T zones were taken from an average temperature profile based on XBT data collected by the R/V LAMB in the study area during the early phase of the experiment. The vertical displacement is computed with respect to a reference or nominal depth. Here the nominal depth is defined as the reference sensor depth for a specific boundary condition of surface tension excluding horizontal displacements of the mooring. Thus the nominal depth includes changes in mooring length due to stretch resulting from changes in total mooring weight. As an example, typical values of surface tension for conditions of strong and moderate forcing are 10^4 and 7×10^3 Kg, respectively. The corresponding nominal depths for the zone 6 reference sensor are 1854.5 and 1843.2 m. For the zero-external forcing state the nominal depth for the zone 6 reference is 1832.1 m. Thus under strong forcing the reference sensor is 22.4 m deeper due to cable stretch. The vertical excursions, Δz, from nominal result from changes in mooring configuration when horizontal forcing is included.

The results of the simulation studies corresponding to the external inputs given in Table 3 are listed by category in Table 5A through C. For the current shear cases (7-9) the depth at the inflection point is in parenthesis.

CASE	(1)		(2)		(3)	
Depth Zone	ΔZ (m)	ΔT (^{o}c)	ΔZ (m)	ΔT (^{o}c)	ΔZ (m)	ΔT (^{o}c)
1	3.75	0.052	1.27	.018	0.16	2.24×10^{-3}
2	8.14	.106	2.82	.037	.37	4.8×10^{-3}
3	17.39	.417	6.25	.150	.86	.021
4	25.57	.307	9.46	.114	1.37	.016
5	35.56	.249	13.58	.095	2.08	.014
6	84.82	.085	36.80	.037	7.35	7.35×10^{-3}

ΔZ: n.nn displacement from nominal (external forcing = 0)

ΔT: (n.nn) γ_T

Table 5A

Environmental Simulation -

Surface and Subsurface Forcing

CASE	(4)		(5)		(6)	
Depth Zone	ΔZ (m)	ΔT (^{o}C)	ΔZ (m)	ΔT (^{o}C)	ΔZ (m)	ΔT (^{o}C)
1	3.87	.054	1.14	.015	.10	1.40×10^{-3}
2	7.41	.096	2.22	.029	.19	2.47×10^{-3}
3	13.56	.325	4.18	.100	.38	9.12×10^{-3}
4	18.34	.220	5.79	.069	.53	6.36×10^{-3}
5	23.79	.166	7.72	.054	.73	5.11×10^{-3}
6	49.71	.050	18.58	.018	2.08	2.08×10^{-3}

ΔZ: n.nn displacement from nominal

ΔT: (n.nn) γ_T

Table 5B

Environmental Simulation -

Surface Forcing - Subsurface Drag = 0

CASE	(7)		(8)		(9)	
Depth Zone	Δ Z (m)	Δ T (^{o}C)	Δ Z (m)	Δ T (^{o}C)	Δ Z (m)	Δ T (^{o}C)
1	2.95	.041	1.96	.027	1.28	.018
2	6.92	.090	4.14	.054	2.51	.033
3	15.75	.378	8.54	.205	4.74	.114
4	23.61	.283	12.36	.148	6.55	.079
5	33.09	.232	17.06	.119	8.67	.061
6	78.56	.078	44.55	.044	19.13	.019

ΔZ : n.nn displacement from nominal

ΔT : (n.nn) γ_T

Table 5c

Environmental Simulation

Surface, Subsurface Forcing - with current shear

3.0 The Vertical Displacement Corrector

This section treats the methodology used to correct the signal of sensors attached along the mooring line for contamination resulting from changes in mooring configuration. The first two parts include 1) the detailed development of the vertical displacement corrector model (VDCM) and 2) the methodology used to compute the vertical displacements of the individual sensors and, subsequently, correction of the sensor signal. The final part of this section examines the model application. Included is 1) a comparison of the configuration computed - VDCM vs MCM - for varying boundary conditions and 2) a comparison of the corrected signal vs XBT measurements.

3.1 General Assumptions and Capabilities

The VDCM is a modified version of the mooring configuration model. The assumptions used to mathematically describe the mooring system are the same as those used for the MCM. The method of solution utilizing the finite element approach is identical as well with the exception of the iteration scheme used to close the solution. The primary difference between the two models is in the approach used to specify the boundary conditions. To recap, the MCM uses explicit inputs of 1) the magnitude of the surface wind, wave, and current to compute the surface forces acting on the buoy and 2) the current profile used to compute the subsurface drag. As such all external forces are given.

For the VDCM, however, the explicit inputs listed above are not available and must be derived using measured

quantities - the cable inclination and tension at the surface and the cable inclination at the junction between the cable and nylon members (approximately at a nominal depth of 1900 m). Given the inclination and tension at the surface the total surface forcing on the buoy can be determined but the components due to wind, wave, and current cannot be separated. As such, in the initial pass the method uses the surface input (inclination and tension) to compute the surface force (total) and solves the set of force-balance equations assuming a no-subsurface drag condition. It should be noted that the solution is unique for a given value of the surface boundary conditions and the solution will converge if and only if the no-drag condition is satisfied. Mathematically the formulation is similar to the catenary problem. Under conditions of zero-subsurface forcing (here defined as the zeroth state) the horizontal tension is constant with depth. It should be pointed out, however, that the inclinations at the surface and 1900 m need not be equal to satisfy the zeroth condition. If the solution does not converge then subsurface drag must be added. Under a drag condition the horizontal tension is not constant with depth. Thus the difference in measured inclination between the surface and 1900 m is proportional to the sum of the drag between those depths and the drag, in turn, is proportional to v^2 (horizontal current speed). To satisfy this condition a current profile is computed which satisfies the drag requirement. A simple linearly-

decreasing profile is assumed.

Formulation of Subsurface Drag and Current Profile

For cases in which the zeroth condition is not satisfied ie., the solution does not converge - this implies that an unknown percentage of the horizontal component of tension is due to drag. The actual current profile is unknown and therefore the distribution of drag with depth. The static formulation is similar to the catenary problem with the exception that under drag conditions the horizontal component of tension for an arbitrary depth Z_i is

$$F_{h,i} = F_{h,s} + \int_{j=1}^{i} F_{dj}\, dz \tag{28}$$

rather than a constant F_h with depth. In Eq. (28) the subscript s denotes the surface. To approximate the integrated drag portion of Eq. (28) the following method is used.

Using the measured line inclinations at the surface, θ_s, and bottom of the thermistor cable, θ_c, the sum of the drag between the surface and cable bottom, Z_c by rewriting Eq. (28) becomes

$$\int_{j=1}^{c} F_{dj}\, dz = F_{h,c} - F_{h,s} \tag{29}$$

For the static case the vertical component of tension at Z_c is simply the weight of the mooring below Z_c. Thus,

$$F_{v,c} = F_{v,s} - \int_{j=1}^{c} (mg)_c \, dz \tag{30}$$

and the tangential tension is:

$$T_c = F_{v,c} \, (\sin \theta_c)^{-1} \tag{31}$$

Therefore, it follows that

$$F_{h,c} = T_c \cos \theta_c \tag{32}$$

As an aside it should be noted at this point that the solution of Eq. (29) provides not only the magnitude of the sum of the drag to Z_c, but also the sign of the integrated current. Thus, the following criteria:

$$\int_{j=1}^{c} F_{dj} \, dz \quad \begin{cases} > 0, & v > 0 \\ = 0, & \text{zeroth case} \\ < 0, & v < 0 \end{cases} \tag{33}$$

As an example, for $v < 0$ the current increases the horizontal component of tension in the negative sense with respect to the surface value. The effect is to reduce the magnitude of the horizontal excursion of the mooring and, in the case of a strong current, can change the direction of the excursion.

At this point no further assumptions have been applied. Since current profiles were not measured the variability of the drag with depth is unknown. Therefore, to simplify

the problem the current profile is assumed to be linearly decreasing with depth from a surface maximum to zero at the ocean bottom.

To reiterate, the drag acting on line segment i is given by Eq. (5) - refer to Section 2.2.

$$F_{di} = \frac{c_d \rho D S_i V_i^2}{2} \sin \theta_i \tag{5}$$

Thus, Eq. (29) can be expressed as

$$\int_{j=1}^{c} F_{dj}\, dz = \frac{c_d \rho D}{2} \int_{j=1}^{c} S_j V_j^2 \sin \theta_j\, dz \tag{34}$$

c_d and line cross-section D are constant and for simplicity changes of density ρ with depth are ignored. From Section 2.5 it was shown that for the cable at 43% load the percent stretch is 1.09% (Table 2). As such, changes in cable length have a negligible effect on the numerical value of Eq. (34). To simplify further, since a linear current profile is assumed the change in inclination, θ_i, is assumed to change linearly from the surface to Z_c. Thus Eq. (34) becomes

$$\int_{j=1}^{c} V_j^2\, dz = \frac{K_o}{D_o} \tag{35}$$

where, we let

K_o denote the numerical difference in horizontal tensions between the surface and Z_c, and

$$D_o = \frac{c_d \rho D S}{2} \sin \bar{\theta} \tag{36}$$

$\bar{\theta}$ is the numerical average taken from the linearly changing θ_i profile and S the line length.

To construct the linear current profile the average value, $\bar{v}$, of the current between the surface and Z_c is at depth $\bar{Z}$ which lies midway between z = 0 and Z_c. To find $\bar{v}$ we assume that

$$\bar{V} = \left[\frac{\int_{j=1}^{c} v_j^2 \, dz}{n_c} \right]^{\frac{1}{2}} = \left(\frac{K_o}{D_o} \cdot n_c \right)^{\frac{1}{2}} \tag{37}$$

where

n_c is the number of segments between Z = 0, Z_c.

The above expression is not, of course, exact but is a close approximation for n_c, large. In the VDCM n_c is generally $\simeq 374$.

Having determined $\bar{V}$, the slope, m_c, of the current profile between $\bar{Z}$ and the ocean bottom, Z_b is

$$m_c = \frac{\bar{v}}{Z_b - \bar{Z}} \tag{38}$$

and the magnitude of the surface current is

$$V_s = \bar{V} + m_c \bar{Z} \tag{39}$$

The sign of V_s is determined using the criteria given by Eq. (33). The VDCM is then run with drag computed using the estimated current profile.

3.2 Method of Solution

The method of solution for the VDCM is the same as utilized by the MCM with the exceptions as developed in the previous section. With the estimated current profile

determined the models are the same except for the iteration method to be given later in this section. Eqs (17) and (18) are used to determine the forces acting on the buoy and Eqs (23) and (24) for the mooring line.

The iteration method is the following. At the end of each iteration the bottom boundary conditions are applied in the same manner as was done with the MCM; ie, Eq. (27) - Section 2.5. For the initial iteration the zeroth state is assumed. If the zeroth criteria are not met the second iteration uses the estimated current profile as given in Section 3.1. Again if the computed depth does not agree to within 0.1% the process is repeated. For the MCM the iteration variable is F_v', but for the VDCM it is Vs and the corresponding computed current profile. As derived in Section 3.1 V_s is a function of $\bar{V}$, Eq. (37), which is an approximation. The force balance formulation is sensitive to small changes in horizontal forcing - eg, Eq. (23) - such that Eq. (37) is used only for the initial estimate on the second iteration. Initial values, V_s, used in subsequent iterations are found by fine - tuning the initial V_s via extrapolation using the following criteria.

$$\begin{aligned}
&\text{For, } (Z_p - Z')_m > |\varepsilon Z'| \quad \text{and} \\
&(Z_p - Z')_m \gtrless 0 \text{ and } < (Z_p - Z')_{m-1}, \Delta V_s < 0 \\
&(Z_p - Z')_m \gtrless 0 \text{ and } > (Z_p - Z')_{m-1}, \Delta V_s > 0
\end{aligned} \tag{40}$$

where,

Z_p is the predicted bottom depth,

Z' is the measured depth, and subscript m the iteration number.

The new initial guess, V_s', is specified by

$$V_s' = V_s + \Delta V_s \tag{41}$$

In application the VDCM is run for each acquisition period. The model outputs the mooring configuration and the computed depth at each sensor location.

Computing Vertical Displacements and Signal Correction

To compute the vertical displacement at each sensor location the computed location depth as returned by the VDCM was substracted from the computed nominal depth. As defined in Section 2.6.2 the nominal depth is the reference at which the sensor would reside in the absence of changes in mooring configuration. As such the sensor signal (temperature) contained fluctuations due both to the environment and to changes in depth. To correct the signal for bias due to depth changes the following method was used.

(1) The change in temperature due to depth changes, ΔT_i

$$\Delta T_i = \bar{\gamma}_T \cdot \Delta z_i \tag{42}$$

$\bar{\gamma}_T$ is the average temperature gradient for the experimental area based on historical data

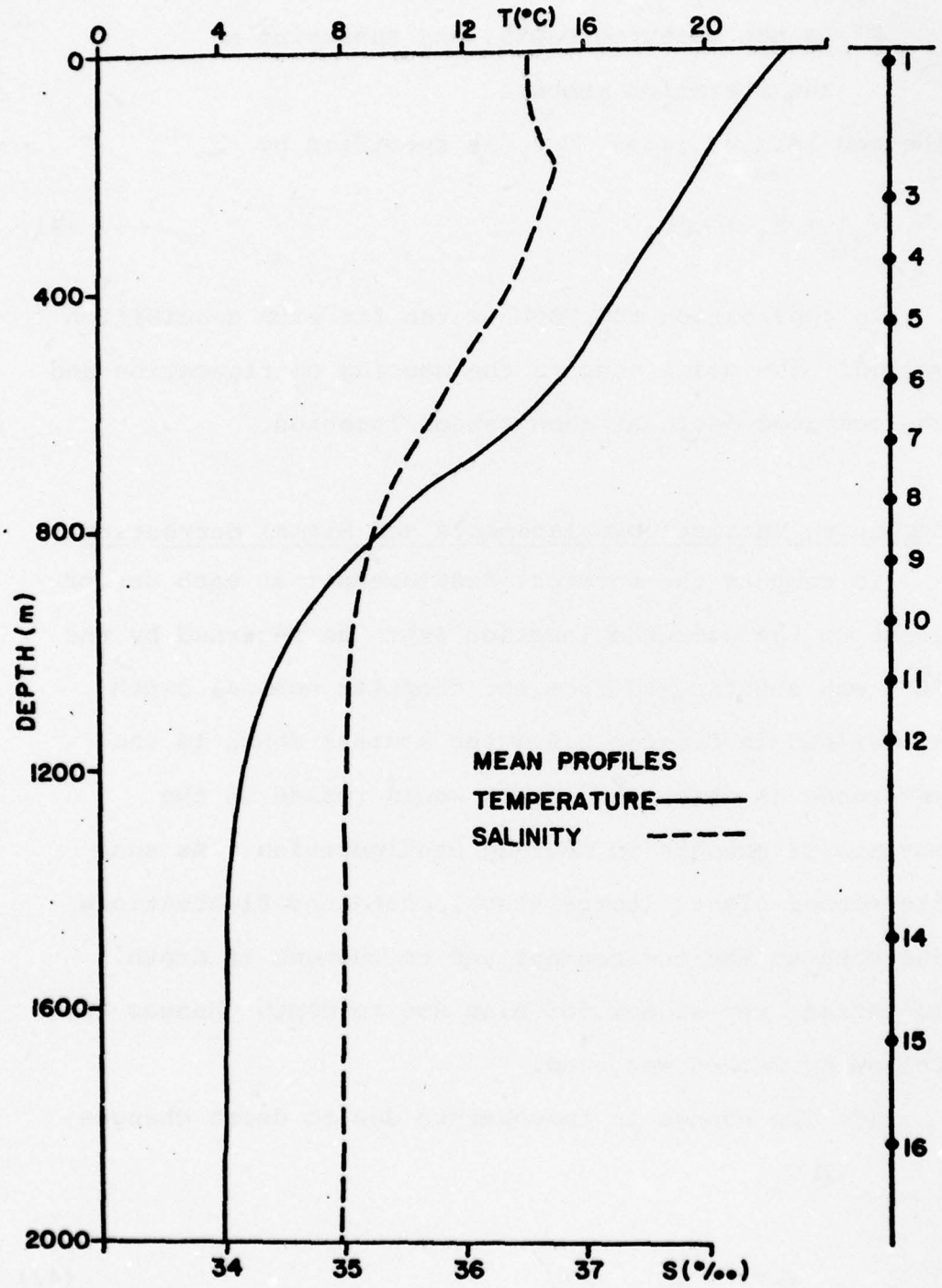

Fig. 8

Mean Profiles, Temperature and Salinity

(FNWC and XBT from the R/V LAMB). The $\bar{\gamma}_T$ used is shown in Fig. 8.

ΔZ_i is the computed depth change from nominal at sensor location i.

(2) In situ temperature, T'

$$T' = T_m - \Delta T_i \tag{43}$$

T_m is the measured temperature not corrected for displacement bias.

3.3 Model Verification - Corrector vs MCM - vs XBT Data

Ideally, verification of the model would include a comparison of model predictions vs environmental measurements over a wide range of environmental conditions. However, for the remote BEAR Buoy system the above approach was not practical. As an alternative, several case studies were conducted to provide environmental data which could be used to evaluate the following.

1) To verify the capability of the model to accurately define the nominal zero-external forcing state.
2) To verify the accuracy of the model in predicting mooring configuration during periods of non-zero external forcing.

The model verification included comparisons of MCM vs tensiometer measurements, MCM vs VDCM results, and VDCM vs XBT measurements.

Nominal Condition

As discussed in Section 2.6.1 the mooring weight was measured during the Ground Truth Experiment. For the

condition of zero-external forcing the measured surface tension is equal to the weight of the mooring which includes the cable and nylon members and a short length of the ground tackle. As such, the measured weight yields the total mooring length with stretch included since the weight per unit length of each member is known. The MCM was run using the measured tension as input. The model prediction of total mooring length (stretch included) agreed with the field measurements within the error limits of the instrumentation used. Conclusion: the model accurately predicts mooring length with elasticity included for the nominal state.

External-Forcing Condition

To test the accuracy of the model in predicting the mooring configuration during the non-zero external forcing state, two study comparisons were made.

1) MCM vs VDCM comparison
2) VDCM vs XBT measurements

MCM vs VDCM Comparison

The MCM and VDCM were compared for several case studies of differing conditions of surface and subsurface forcing. Table 3 (Section 2.6.2) summarizes the inputs for each case. For the MCM/VDCM comparison cases 7-9 were not run. The

	(1)			(2)			(3)		
Depth Zone	ΔZ (m)	ΔT (^oC)	ΔTE_r (^oC)	ΔZ (m)	ΔT (^oC)	ΔTE_r (^oC)	ΔZ (m)	ΔT (^oC)	ΔTE_r (^oC)
1	3.75 (3.73)	.052	2.8×10^{-4}	1.27 (1.26)	.018	1.4×10^{-4}	0.16 (0.16)	2.24×10^{-3}	0.
2	8.14 (8.08)	.106	7.8×10^{-4}	2.82 (2.78)	.037	5.2×10^{-4}	0.37 (0.35)	4.8×10^{-3}	2.6×10^{-4}
3	17.39 (17.23)	.417	3.8×10^{-3}	6.25 (6.14)	.150	2.64×10^{-3}	0.86 (0.82)	.021	9.6×10^{-4}
4	25.57 (25.31)	.307	3.12×10^{-3}	9.46 (9.26)	.114	2.4×10^{-3}	1.37 (1.30)	.016	8.4×10^{-4}
5	35.56 (35.16)	.249	2.8×10^{-3}	13.58 (13.26)	.095	2.24×10^{-3}	2.08 (1.95)	.014	9.1×10^{-4}
6	84.82 (83.76)	.085	1.06×10^{-3}	36.80 (35.78)	.037	1.02×10^{-3}	7.35 (6.78)	7.35×10^{-3}	5.7×10^{-4}

ΔZ : n.nn displacement from nominal - MCM

(n.nn) displacement from nominal - VDCM

ΔT : n.nn$\cdot\gamma_T$

ΔTE_r: $\{n.nn - (n.nn)\} \cdot \gamma_T$

Table 6A

Surface and Subsurface Forcing

	(4)			(5)			(6)		
Depth Zone	ΔZ (m)	ΔT (^oC)	ΔTE_r (^oC)	ΔZ (m)	ΔT (^oC)	ΔTE_r (^oC)	ΔZ (m)	ΔT (^oC)	ΔTE_r (^oC)
1	3.87 (3.87)	.054	0.	1.14 (1.14)	.016	0.	0.10 (0.10)	1.40×10^{-3}	0.
2	7.41 (7.41)	.096	0.	2.22 (2.22)	.029	0.	0.19 (0.19)	2.47×10^{-3}	0.
3	13.56 (13.55)	.325	2.4×10^{-4}	4.18 (4.18)	.100	0.	0.38 (0.38)	9.12×10^{-3}	0.
4	18.34 (18.33)	.220	1.2×10^{-4}	5.79 (5.78)	.069	1.2×10^{-4}	0.53 (0.53)	6.36×10^{-3}	0.
5	23.79 (23.79)	.166	0.	7.72 (7.71)	.054	7.0×10^{-5}	0.73 (0.73)	5.11×10^{-3}	0.
6	49.71 (49.70)	.050	1.0×10^{-5}	18.58 (18.56)	.018	1.0×10^{-5}	2.08 (2.09)	2.08×10^{-3}	1.0×10^{-5}

Table 6B

Surface Forcing - Subsurface Drag = 0

thermistor displacement (referenced to the zero forcing - nominal state) for each sensor location was computed by both the MCM and VDCM and compared for each case study. Tables 6A and B summarize, respectively, the results for surface plus subsurface forcing and for surface forcing - zero subsurface drag cases. For the sake of brevity, only one sensor location was chosen for each of six depth zones defined in Table 4 (Section 2.6.2). In Tables 6A and B, ΔZ represents the vertical displacement (m) of the thermistor from the nominal (zero force) depth position. The ΔT represents the temperature differential due to vertical displacement - referenced to the MCM prediction and ΔTE_r is the difference in differential temperatures between the MCM and VDCM. As seen in Table 6B the error is essentially zero since there is no ambiguity between the two models for the zero subsurface drag case.

In the comparison given, the depth zones (Table 4) represent regions of average gradient. In actual practice the gradients are obtained from the average temperature profile over a much smaller vertical distance - generally of the order of the nominal depth (thermistor N) +100 m, maximum. In comparing these values with ΔTE_r it should be noted that the error between the MCM and VDCM is less that the resolution (^{o}c/bit) of the thermistors used.

VDCM vs XBT Measurements

The model results using acquired data were compared with XBT measurements collected by the R/V LAMB. During the acquisition period the surface conditions were moderate to strong - no current measurements were made. The data used for the comparison study were the temperature values - uncorrected and corrected for vertical displacements. Fig. 9 and Table 7 give the results. The percent difference, $\%\Delta$, between the XBT and buoy data are given in columns 4 and 6 - Table 7 - for the uncorrected and corrected measurements, respectively. The VDCM reduces the $\%\Delta$ by a factor of three for the given conditions of external forcing.

In the case study presented above the XBT measurement was used as the reference assuming no instrumental error. As an aside the BEAR data - corrected for vertical displacement - were compared with XBT data corrected for an assumed bias. In a study conducted for the U.S. Coast Guard, Gaillard et al (1970) showed the standard sippican XBT to have a response bias of 4.57 m or 2% assuming a drop rate of 5.08 ms^{-1}. The XBT measurement used in this study was corrected for the above bias (given in column 7, Table 8) and compared with the buoy data. The reduction in percent difference (column 8) is very slight - the order of 1% maximum.

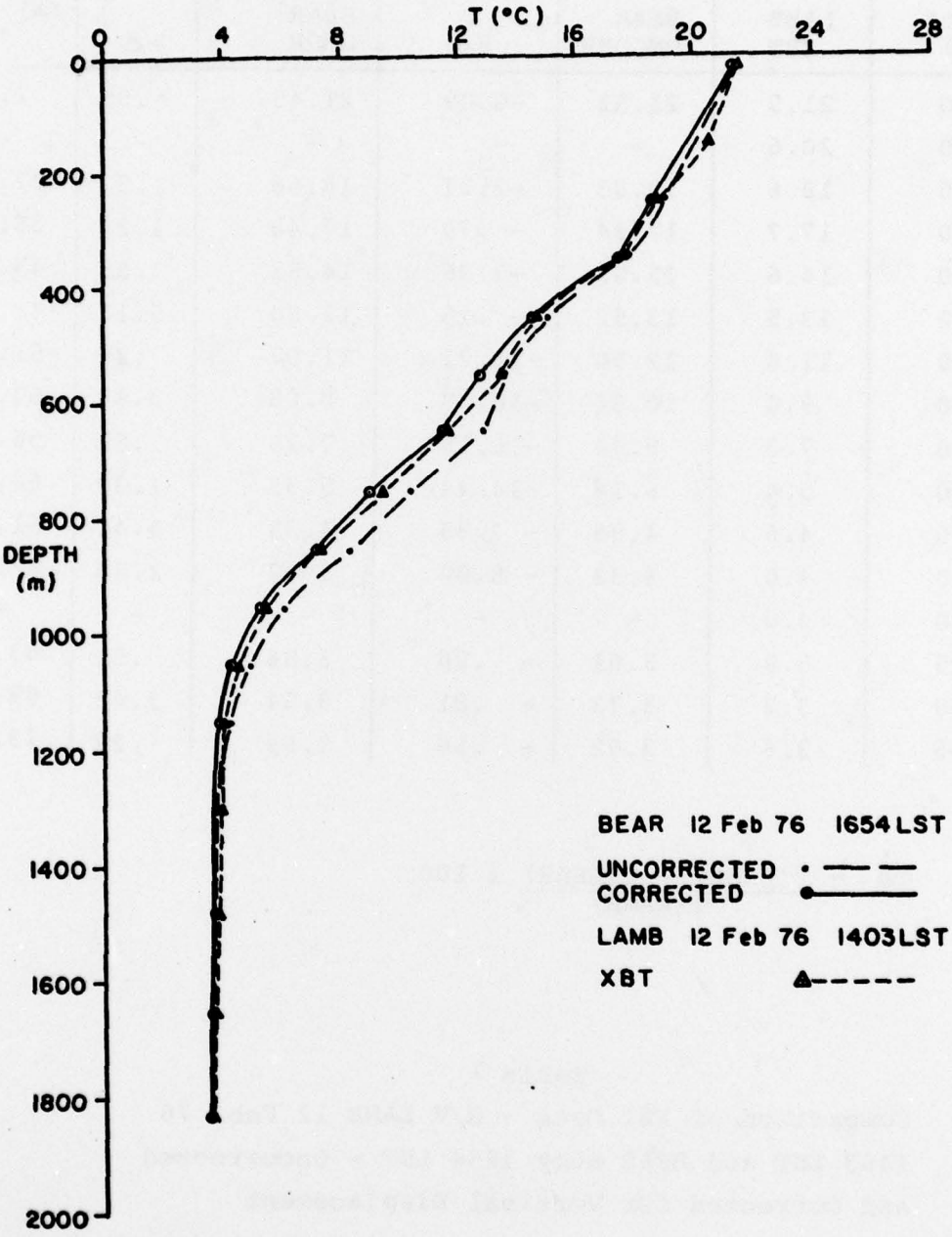

Fig. 9

Model Results vs XBT Comparison

1	2	3	4	5	6	7	8
	T(°C)			T(°C)		ΔZ CORR	γ_T °C/m
Depth (m)	LAMB XBT	BEAR UNCORR	%Δ	BEAR CORR	%Δ	(m)	
20	21.5	21.52	-0.09	21.49	.05	2.7	.0100
150	20.6	-	-	-	-	-	-
250	18.6	19.03	-2.31	18.66	- .32	27.8	.0133
350	17.7	17.84	- .79	17.48	1.24	36.0	.0100
450	14.6	15.09	-3.36	14.52	.55	45.6	.0125
550	13.5	13.52	- .15	12.80	5.18	48.0	.0150
650	11.6	12.90	-11.21	11.57	.26	51.2	.0260
750	9.4	10.34	-10.00	9.08	3.40	54.1	.0233
850	7.3	8.48	-16.16	7.25	.68	56.7	.0217
950	5.4	6.18	-14.44	5.33	1.30	60.7	.0140
1050	4.6	4.96	- 7.83	4.35	5.44	61.0	.0100
1150	4.0	4.32	- 8.00	3.92	2.00	62.5	.0064
1300	4.0	-	-	-	-	-	-
1475	3.9	3.91	- .26	3.88	.51	63.9	.0036
1650	3.7	3.73	- .81	3.64	1.62	69.2	.0013
1825	3.6	3.62	- .56	3.59	.28	73.2	.00041

$$\%\Delta = \frac{T(LAMB) - T(BEAR)}{T(LAMB)} \times 100$$

Table 7

Comparison of XBT Data - R/V LAMB 12 Feb. 76 1403 LST and BEAR Buoy 1654 LST - Uncorrected and Corrected for Vertical Displacement

1	2	3	4	5	6	7	8	9
							XBT CORR	
Depth (m)	T(°C) XBT	T(°C) BEAR	%Δ	∇T (°C/m)	ΔT	T(°C) XBT CORR	%Δ BEAR CORR	%Δ BEAR UNCORR
20	21.5	21.49	.05	.0100	.04	21.46	-.14	- .28
150	20.6	-	-	-	-	-	-	-
250	18.6	18.66	-.32	.0133	.06	18.54	-.65	-2.64
350	17.7	17.48	1.24	.0100	.04	17.66	1.02	-1.02
450	14.6	14.52	.55	.0125	.06	14.54	.14	-3.78
550	13.5	12.80	5.18	.0150	.07	13.43	4.69	-.67
650	11.6	11.57	.26	.0260	.12	11.48	-.78	-12.37
750	9.4	9.08	3.40	.0233	.11	9.29	2.26	-11.30
850	7.3	7.25	.68	.0217	.10	7.20	-.69	-17.78
950	5.4	5.33	1.30	.0140	.06	5.34	.19	-15.73
1050	4.6	4.35	5.44	.0100	.04	4.56	4.60	- 8.77
1150	4.0	3.92	2.00	.0064	.03	3.97	1.26	- 8.82
1300	4.0	-	-	-	-	-	-	-
1475	3.9	3.88	.51	.0036	.02	3.88	0.	- .77
1650	3.7	3.64	1.62	.0013	.01	3.69	1.36	- 1.08
1825	3.6	3.59	.28	.00041	0.	3.60	.28	- .56

Table 8

VDCM Corrected Data vs XBT -
XBT Bias Assumed

4.0 Summary

This study has presented the mathematical development of the mooring configuration model (MCM) and the vertical displacement corrector model (VDCM).

The MCM uses explicitly the surface forces (due to wind, wave, and current) and subsurface drag (due to current) to compute the configuration of the mooring. The VDCM, on the other hand, uses the total measured surface tension and approximates the subsurface drag using as inputs the mooring instrumentation measurements - tension and line inclination at the surface and inclination at the cable, nylon junction. The MCM is used exclusively to analyze mooring configuration for specific case studies of external forcing. The VDCM is used to correct the measured temperature values for bias due to vertical displacements.

Comparison of model results (MCM vs VDCM) have shown the method used to approximate the subsurface drag to be valid and to yield results consistent with the MCM. Comparison of VDCM vs XBT measurements have shown that the VDCM reduces the error between buoy and XBT data by as large as a factor of three for conditions of moderate to strong external forces.

REFERENCES

1. Casarella, M.J. and M. Parsons, 1970. A survey of investigations on the configuration and motion of cable systems under hydrodynamic loading. Marine Technology Soc. J., 4, 27-43.
2. Dean, R.G. and D.R.F. Harleman, 1968. Interaction of structures and waves. In Estuary and Coastline Hydrodynamics, Ch. 8, A.T. Ippen, Ed., McGraw-Hill, 744 pp.
3. Echternacht, K.L., 1976: BEAR Buoy Ground-Truth Experiment. IAR Tech. Memo, 23 Mar. 1976.
4. Gaillard, R.J., K.I. Heldebrandt, R.M. Crosby and T. Cass, 1970. U.S. Coast Guard Oceanographic Sensor Study - Vol. II State-of-the-Art of Oceanographic and Meteorological Sensors - Catalog. Texas Instruments Inc., 21 May 1970.
5. Hartman, P.J. and C.D. Nash, Jr., 1975. Current profile strength and its effect on mooring reliability. MTS Journ., 9, 33-38.
6. Langer, R.M., 1974: The catenary in space-free motions of flexible lines. J.R.M. Bege Co., AD 611429, Defense Documentation Center.
7. Morrow, B.W. and W.F. Chang, 1967: Determination of the optimum scope of a moored buoy. Jour. of Ocean Tech., 2, 37-42.
8. Pode, L., 1951: Tables for computing the equilibrium configuration of a flexible cable in a uniform stream. Report 687, David Taylor Model Basin.

9. Reid, R.O., 1968: Dynamics of deep-sea mooring lines. A and M Project 204, Ref. 68-11F, Dept. of Oceanog. Texas A and M Univ., College Station, Texas.

10. Walton, T.S. and H. Polachek, 1959: Calculations on non-linear transient motion of cables. David Taylor Model Basin, Applied Math. Lab. Report No. 1279.

11. Wilson, B., 1961: Characteristics of deep sea anchor cables in strong ocean currents. Texas A and M Tech. Report No. 203-3, Dept. of Oceanog. and Meteorology.

12. _____, and D.H. Garbaccio, 1967: Dynamics of ship anchor lines in waves and currents. Proc. of the Conf. on Civil Eng. in the Oceans, Am. Soc. of Civil Eng., San Francisco.

13. Wunsch, C. and J.M. Dahlen, 1974: A moored temperature and pressure recorder. Deep-Sea Res., 21, 145-154.

DISTRIBUTION LIST

Director 1
Office of Naval Research Branch Office
1030 East Green Street
Pasadena, California 91106

Office of Naval Research 1
San Francisco Area Office
760 Market Street - Room 447
San Francisco, California 94102

Director 1
Office of Naval Research Branch Office
495 Summer Street
Boston, Massachusetts 02210

Director 1
Office of Naval Research Branch Office
536 South Clark Street
Chicago, Illinois 60605

Commanding Officer 8
Office of Naval Research Branch Office
Box 39
FPO New York 09510

Commander 1
Naval Ordnance Laboratory
Acoustics Division
White Oak
Silver Spring, Maryland 20910
Att: Dr. Zaka Slawsky

Office in Charge 1
Annapolis Laboratory
Naval Ship Research and Development Center
Annapolis, Maryland 21402

Defense Documentation Center 10
Cameron Station
Alexandria, Virginia 22314

Superintendent 1
Naval Academy
Annapolis, Maryland 21402

Commanding Officer 1
Naval Intelligence Support Center
4301 Suitland Road
Washington, D.C. 20390
Att: Dr. Johann Martinek
Mr. E. Bissett

Commander
Naval Sea Systems Command
Code SEA 03E
Washington, D.C. 20362 — 1

Dr. Charles Stutt
General Electric Company
P.O. Box 1088
Schenectady, New York 12301 — 1

Dr. Harry DeFerrari
University of Miami
Rosenstiel School of Marine and
Atmospheric Science
Miami, Florida 33149 — 1

Mr. Robert Cunningham
Bendix Electronics Center
15825 Roxford Street
Sylmar, California 91342 — 1

Dr. Stephen Wolff
John Hopkins University
Baltimore, Maryland 21218 — 1

Dr. M.A. Basin
S.D.P., Inc.
15250 Ventura Blvd., Suite 518
Sherman Oaks, California 91403 — 1

Dr. Walter Duing
University of Miami
Rosenstiel School of Marine and
Atmospheric Science
Miami, Florida 33149 — 1

Dr. David Middleton
127 East 91st Street
New York, New York 10028 — 1

Dr. Donald W. Tufts
University of Rhode Island
Kingston, Rhode Island 02881 — 1

Dr. Loren W. Nolte
Dept. of Electrical Engineering FT-10
University of Washington
Seattle, Washington 98195 — 1

Mr. S.W. Autrey
Hughes Aircraft Company
P.O. Box 3310
Fullerton, California 92634 — 1

Dr. Thomas W. Ellis
Texas Instruments, Inc.
13500 North Central Expressway
Dallas, Texas 75231 — 1

Mr. Robert Swarts 1
Applied Physics Laboratory
University of Washington
1013 N.E. 40th Street
Seattle, Washington 98195

Mr. Charles Loda 1
Institute for Defense Analyses
400 Army-Navy Drive
Arlington, Virginia 22202

Mr. Beaumont Buck 1
Polar Research Laboratory
123 Santa Barbara Avenue
Santa Barbara, California 93101

Dr. M. Weinstein 1
Underwater Systems, Inc.
8121 Georgia Avenue
Silver Spring, Maryland 20910

Dr. Thomas G. Kincaid 1
General Electric Company
P.O. Box 1088
Schenectady, New York 12301

Applied Research Laboratories 4
The University of Texas at Austin
P.O. Box 4029
Austin, Texas 78712
Att: Dr. Lloyd Hampton
Dr. Charles Wood
Dr. T.D. Plemons

Woods Hole Oceanographic Institute 1
Woods Hole, Massachusetts 02543
Att: Dr. Paul McElroy
Mr. R. Porter
Mr. R. Spindel

Dr. John Bouyoucos 1
Hydroacoustics, Inc.
321 Northland Avenue
P.O. Box 3818
Rochester, New York 14610

Systems Control, Inc. 1
260 Sheridan Avenue
Palo Alto, California 94306
Att: Mr. Robert Baron

Dr. David Hyde 1
Special Assistant (Electronics)
Office of the Assistant
Secretary of the Navy
R&D Pentagon
Washington, D.C. 20350

CDR. Harry C. Furminger, USN 1
Commanding Officer
U.S. Naval Facility
FPO, New York 09556

Dr. Victor C. Anderson 1
Marine Physical Laboratory
Scripps Institution of Oceanography
University of California
La Jolla, Calif. 92037

UNCLASSIFIED

SECURITY CLASSIFICATION OF THIS PAGE (When Data Entered)

REPORT DOCUMENTATION PAGE	READ INSTRUCTIONS BEFORE COMPLETING FORM
1. REPORT NUMBER: IAR-77008	2. GOVT ACCESSION NO. / 3. RECIPIENT'S CATALOG NUMBER
4. TITLE (and Subtitle): BEAR Buoy: The Mooring Configuration Model and Method Used to Correct Sensors for Vertical Displacement.	5. TYPE OF REPORT & PERIOD COVERED: Final Report, 1 Nov 76 - 31 Dec 77
	6. PERFORMING ORG. REPORT NUMBER
7. AUTHOR(s): Kenneth L. Echternacht	8. CONTRACT OR GRANT NUMBER(s): N00014-74-C-0229
9. PERFORMING ORGANIZATION NAME AND ADDRESS: Institute for Acoustical Research, 615 S.W. 2nd Avenue, Miami, Florida 33130	10. PROGRAM ELEMENT, PROJECT, TASK AREA & WORK UNIT NUMBERS
11. CONTROLLING OFFICE NAME AND ADDRESS: Procuring Contracting Officer, Office of Naval Research, Dept. of the Navy, Arlington, Va. 22217	12. Dec 77 / 13. NUMBER OF PAGES: 68 p.
14. MONITORING AGENCY NAME & ADDRESS (if different from Controlling Office): Office of Naval Research Resident Rep., Columbia University, Lamont Doherty Geological Observatory, Torrey Cliff, Palisades, New York 10913	15. SECURITY CLASS. (of this report): Unclassified / 15a. DECLASSIFICATION/DOWNGRADING SCHEDULE

16. DISTRIBUTION STATEMENT (of this Report)

Distribution of this Document is unlimited

17. DISTRIBUTION STATEMENT (of the abstract entered in Block 20, if different from Report)

18. SUPPLEMENTARY NOTES

19. KEY WORDS (Continue on reverse side if necessary and identify by block number)

Buoy measurements, temperature, mooring configuration, correction for vertical displacements

(AD-A051 517)

20. ABSTRACT (Continue on reverse side if necessary and identify by block number)

This report constitutes Part 2 of a two part report. Part 1 "BEAR Buoy: The Engineering Documentation for Scientific Application", dealt with details of the system design and calibration. This report first, develops the mathematical model used to determine the mooring configuration for varying conditions of external forcing. Second, the method used to correct sensors (thermistors) for vertical displacements is presented. Included → over

DD FORM 1 JAN 73 1473 EDITION OF 1 NOV 65 IS OBSOLETE S/N 0102-014-6601

UNCLASSIFIED

SECURITY CLASSIFICATION OF THIS PAGE (When Data Entered)

408 141

are case study comparisons of the model predictions vs actual measurements.